Title

Photochemical Diodes for Simultaneous Bias-Free Glycerol Valorization and Hydrogen Evolution

Journal

Journal of the American Chemical Society, 145(24)

ISSN

0002-7863

Authors

Lin, Jia-An
Roh, Inwhan
Yang, Peidong

Publication Date

2023-06-21

DOI

10.1021/jacs.3c01982

Peer reviewed

Photochemical Diodes for Simultaneous Bias-free Glycerol Valorization and Hydrogen Evolution

Jia-An Lin[†,‡,⊥], Inwhan Roh[†,‡,⊥] and Peidong Yang[†,‡,§,||,#,*]

[†]Department of Chemistry, University of California, Berkeley, California 94720, United States
[‡]Liquid Sunlight Alliance, Lawrence Berkeley National Laboratory, Berkeley, California, 94720, United States
[§]Department of Materials Science and Engineering, University of California, Berkeley, California 94720, United States
[||]Chemical Sciences Division, Lawrence Berkeley National Laboratory, Berkeley, California 94720, United States
[#]Kavli Energy NanoScience Institute, Berkeley, California 94720, United States
*p_yang@berkeley.edu

Supporting Information Placeholder

ABSTRACT: Artificial photosynthesis offers a route to produce clean fuel energy. However, the large thermodynamic requirement for water splitting along with the corresponding sluggish kinetics for the oxygen evolution reaction (OER) limit its current practical application. Here, we offer an alternative approach by replacing OER with the glycerol oxidation reaction (GOR) for value added chemicals. By using a Si photoanode, low GOR onset potentials of -0.05 V vs. RHE and photocurrent densities of 10 mA/cm^2 at 0.5 V vs. RHE can be reached. Coupled with a Si nanowire photocathode for the hydrogen evolution reaction (HER), the integrated system yields high photocurrent densities of 6 mA/cm^2 with no applied bias under 1 sun illumination and can run for over 4 days under diurnal illumination. The demonstration of the GOR-HER integrated system provides a framework for designing bias-free photoelectrochemical devices at appreciable currents, and establishes a facile approach toward artificial photosynthesis.

Finding sustainable and renewable energy is currently one of the most urgent challenges facing society today.[1–3] With the sun providing 173 PW to the Earth's surface every year, or enough energy in one hour to match the world's yearly energy consumption[4], artificial photosynthesis offers an attractive route to using solar energy to produce fuels such as hydrogen, a fundamental component for building a carbon-free economy.[2,5,6] One such approach to realize artificial photosynthesis is presented through the photochemical diode.[7,8] Photoanodes and photocathodes can be integrated through an ohmic contact, coupling both oxidative and reductive half-reactions in a single device.[9–11] Conventional approaches targeted optimizing the overall water splitting (OWS) reaction in which hydrogen and oxygen is produced. However, the sluggish kinetics of OER and the high thermodynamic potential requirement of 1.23 V for OWS limit the current performance of bias-free photoelectrochemical (PEC) systems to ~3.5 mA/cm^2.[12,13] Given that 90% of the overall energy requirements come from OER,[14] alternative oxidative reactions could enable more efficient PEC systems.

As one such strategy, the oxidation of biomass-derived, organic compounds has been proposed as an alternative to OER. These oxidative reactions have low potential requirements (< 0.3 V vs RHE), showing potential reductions up to ~1 V in electrochemical cells when replacing OER.[14,15] Of such compounds, glycerol, the main by-product from biodiesel production, can also electrochemically produce products such as glyceraldehyde (GLD), dihydroxyacetone (DHA), glyceric acid (GLA), and lactic acid (LA), which are widely used in the cosmetics,

pharmaceutical, and food industries[14,16–22] The value of its products and its low potential requirement makes the glycerol oxidation reaction (GOR) an attractive pursuit.

The lower potential requirement of GOR also opens up the avenue for lower photovoltage materials in the photochemical diode design. **Figure 1a** shows the redox potentials of HER, OER, and GOR, as well as the band diagram of typically used photoelectrodes such as Si, TiO_2 and $BiVO_4$. For OWS, the redox potential of OER as well as the 1.23 V potential requirement often meant that metal oxides were favored as photoanode materials due to their wide bandgaps supplying >1 eV of photovoltage and ability to stack on top of small bandgap materials.[9,10,23] However, maximum photocurrents for wide bandgap materials are limited, TiO_2 and $BiVO_4$ supplying 2 and 5 mA/cm^2 respectively (**Figure 1b**).[23–26]

Compared to OWS, GOR coupled with HER reduces the energy requirement by 700-1000 mV allowing for smaller bandgap materials with larger photocurrents to be used (**Figure 1b**).[27,28] Additionally, selectivity can be steered by choosing a semiconductor material like Si where the valence band maximum (VBM) lies in between the potentials for GOR and OER, preventing any holes from being used for OER. In this design framework, a selective bias-free device can be achieved by coupling a medium bandgap material such as silicon with a low onset potential catalyst for GOR.

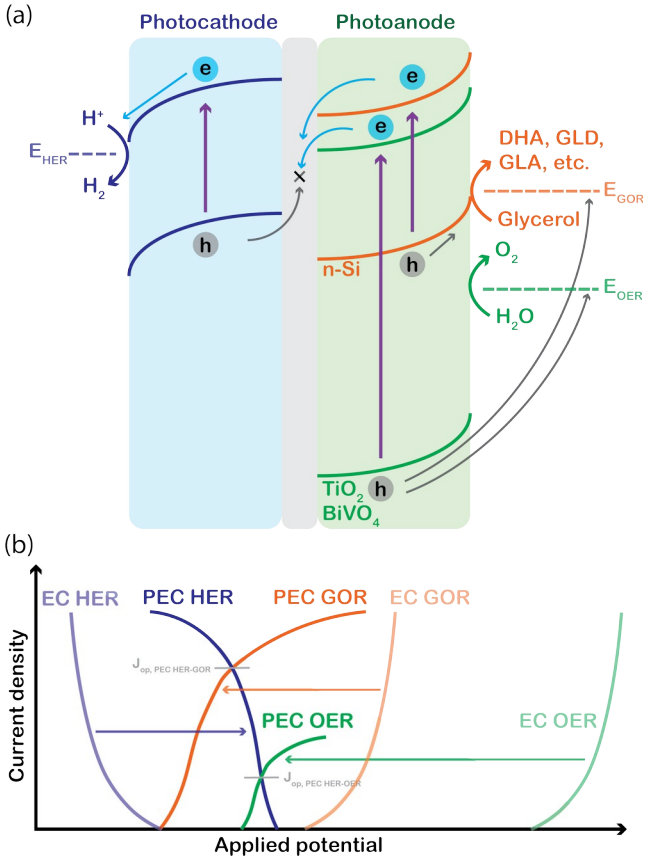

Figure 1. Schematic illustration of using GOR as an alternative to OER within a photochemical diode system. (a) Energy band diagram of photoelectrodes for HER, OER and GOR. The photogenerated electrons in photocathode perform HER while the holes in the photoanode perform GOR and/or OER. Concomitantly, majority carriers recombine at the ohmic contact. (b) Current-voltage curves of electrochemical (EC) and PEC HER, GOR, and OER. Predicted operating photocurrent density of bias-free systems are shown for PEC HER-GOR ($J_{op,\ PEC\ HER\text{-}GOR}$) and HER-OER ($J_{op,\ PEC\ HER\text{-}OER}$).

Prior to photoelectrochemical experiments, it is necessary to find a suitable catalyst with low onset potentials toward GOR. Pt, commonly used for alcohol oxidation, shows a low onset potential of 0.5 V vs RHE (**Figure 2a**) with a peak at 0.84 V vs. RHE. However, Pt becomes readily poisoned by CO-like intermediates[16], dropping the current from 10 to 1 mA/cm^2 at 0.84 V vs. RHE within a few minutes (**Figure 2b, S1**). On the other hand, Au has a low binding energy to CO which prevents CO poisoning and can maintain high current densities for GOR (**Figure 2b, S1**).[16] However, Au shows significantly larger overpotentials with an onset of over 0.9 V vs. RHE. The limitations

of both materials can be mitigated by combining the advantages of Pt and Au synergistically. Using a co-sputtered PtAu thin film, the onset potential toward GOR is 0.4 V vs. RHE, which is 1 V lower than state-of-the-art catalysts for OER (**Figure 2a**). PtAu shows enhanced current densities at low potentials, and a steady state current of 10 mA/cm^2 at 0.84 V vs. RHE (**Figure 2a, b** and **Figure S1**). It also shows both peaks at 0.84 and 1.3 V vs. RHE, this being shifted to higher potentials possibly by its bimetallic nature offering oxide resistance,[29] that indicates the synergistic effects between both metals.

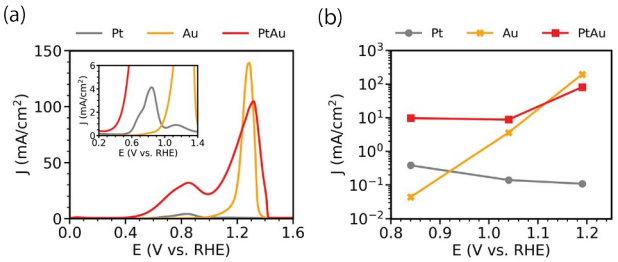

Figure 2. Electrocatalytic performances of Pt, Au, and PtAu. (a) Linear sweep voltammetry (LSV) scans of Pt, Au, and PtAu. Inset is the zoomed-in LSV scans. (b) Steady state current densities of Pt, Au, and PtAu at different potentials. Experiments done in 1 M KOH + 1 M glycerol.

For PEC measurements, 4 nm of PtAu was sputtered onto a TiO_2 protected p$^+$n-Si wafer (**Figure 3a, S2**). TiO_2 is a commonly used passivation layer to protect the silicon surface from corrosive alkaline environments.[30] The surface p$^+$ layer is formed to increase the photovoltage and to enhance the band bending near the semiconductor surface.[31,32] A thin catalyst layer is also required due to the front wet-side illumination geometry. 4 nm is found to be the optimized thickness of PtAu as thinner layers show reduced performance which can be attributed to a decreased amount of active catalyst while thicker layers start to decrease photocurrents by reflecting a significant portion of light (**Figure S3**). **Figure 3b** shows the PEC GOR performance of the PtAu/TiO_2/p$^+$n-Si (referred to as PtAu/Si onwards) photoanode under 100 mW/cm^2 of air mass (AM) 1.5 simulated sunlight in 1 M KOH + 1 M glycerol. The onset potential is around -0.05 V vs. RHE and reaches 10 mA/cm^2 at a potential of 0.5 V vs. RHE which is the lowest overpotential and highest current density reported for PEC GOR (**Table S1**). A strongly alkaline solution causes the first deprotonation step to be base catalyzed due to glycerol (pK_a of ~14) acting as a weak acid. The deprotonated species has been found to be significantly more reactive[33] which is corroborated by our experiments using neutral and acidic electrolytes (**Figure S4**).

The product distribution of PtAu/Si is shown in **Figure 3c**. At 0.34 V vs. RHE, the main products that are produced are GLA with a faradaic efficiency (FE) of 48.1 ± 2.3% and LA with FE of 27.3 ± 2.8% with total products reaching around an FE_{total} of ~80%. The rest likely comes from additional products such as tartronic acid and carbonate (coming from the oxidation of formic acid[34]) that are not analyzable through 1H NMR. Additionally, both DHA and GLD rearranges itself to LA in alkaline electrolytes[35] (**Figure S5**) making it difficult to differentiate production of these compounds versus LA. The product distribution is similar to previously reported electrochemical GOR results using PtAu catalyst under similar conditions.[36] PEC control experiments (**Figure S6**) indicate almost no photocurrent, indicating that glycerol is being oxidized on the PtAu surface.

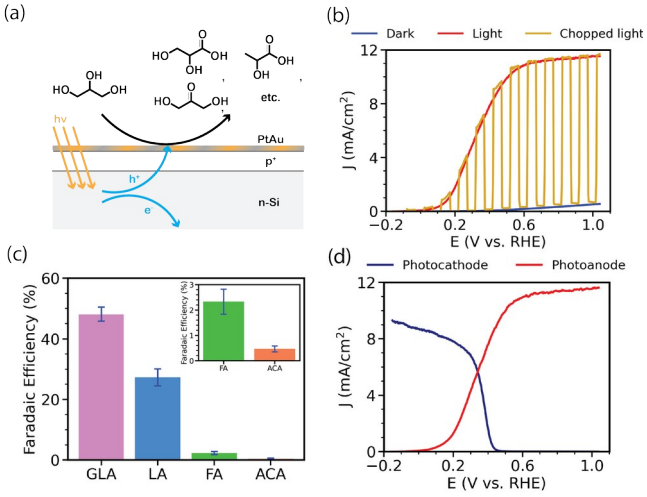

Figure 3. Photoelectrochemical performance of the PtAu/Si photoanode. (a) Schematic of the PtAu/Si photoanode showing dopant layer and electron-hole separation. (b) LSV scans of photoanode under chopped, continuous, and no illumination in 1 M KOH + 1 M glycerol. (c) Selectivity of PEC GOR using PtAu/Si photoanode at 0.34 V vs. RHE under illumination. Error bars are from three independent measurements. Inset is the

zoomed-in selectivity toward formic acid (FA) and acetic acid (ACA). (d) LSV scans showing absolute current density of PtAu/Si photoanode in 1 M KOH + 1 M glycerol and Pt/SiNW photocathode in 0.5 M H_2SO_4 under 1 sun illumination.

As described earlier, metal oxides are often utilized as photoanodes due to their stability, wide bandgap, large photovoltages, and deep VBM level. Surprisingly, despite these advantages and the reduced energy requirement of GOR compared to that of OER, past reports on PEC performances of GOR on these metal oxides are either comparable to OER or have higher onset potentials[24–27,37–39], all of which have onset potentials of 200-400 mV more positive than this current work (**Table S1**). When using the same catalyst on TiO_2, the onset potentials and fill factors remain worse than when Si is used (**Figure S7**). One possible reason could be the poor hole transfer from the VBM to glycerol due to inadequate band alignment. The VBM levels of metal oxides such as TiO_2 and $BiVO_4$ are 2.7 eV and 2.1 eV vs. NHE, respectively,[40,41] which is 2-2.5 eV below the redox potential of GOR. On the other hand, the VBM of silicon with a donor concentration of 10^{15} cm^{-3} is around 0.42 eV vs. NHE which matches the potential for GOR closely and also prevents OER from occuring.[42,43]

The low onset potential and large photocurrent density makes PtAu/Si a suitable photoanode candidate to form a bias-free integrated PEC system. In this demonstration, we use a Pt/TiO2/n^+p-Si nanowire array (referred to as Pt/SiNW onwards) as the photocathode for HER for its low overpotential and high catalytic performance.[31] The photocathode is tested in 0.5 M H_2SO_4 using the same illumination conditions. **Figure 3d** shows the overlap of the J-V PEC linear scans of the PtAu/Si photoanode and Pt/SiNW photocathode where the expected current at no applied bias is seen at the intersection of the two curves. The large current density of 6 mA/cm^2 at the intersection suggests the feasibility of the bias-free PEC system.

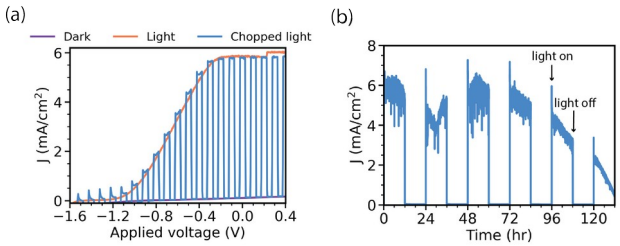

Figure 4. Photoelectrochemical performance of the integrated system of PtAu/Si photoanode and Pt/SiNW photocathode in a two-electrode configuration. (a) LSV scans under chopped, illumination and no illumination. (b) Bias-free diurnal stability test cycling between 12 hours illuminated and 12 hours dark. The fluctuation in current density can be attributed to generation of hydrogen gas bubbles on the photocathode surface.

For the solar driven bias-free integrated PEC system, the photoelectrodes were placed into a two-chamber cell separated by a bipolar membrane (BPM) in a two-electrode configuration (**Scheme S1**). A BPM allows two different pH environments to be used since an alkaline environment is optimal for GOR while an acidic environment is optimal for HER. BPMs also reduce crossover between the electrolytes, preventing reduction of the oxidized products from GOR.[44,45] The integrated system shows an onset potential at around -1.2 V and a photocurrent density up to 6 mA/ cm^2 at zero applied bias (**Figure 4a**) with near unit H_2 selectivity (**Figure S8**), corresponding to 112 $\frac{\mu mol\, H_2}{h \cdot cm^2}$. This agrees well with the expected photocurrent density based on **Figure 3d** showing that the voltage drop across the membrane is 0.83 V.[46,47]

The stability of this bias-free GOR-HER system was also tested using diurnal cycling which mimics the natural sunlight cycle. Potential switching due to light cycling often induces corrosion mechanisms not seen under constant illumination conditions such as rapid etching of the semiconductor or dissolution of the catalyst.[48,49] Our system was able to maintain a high photocurrent density of over 4 mA/cm^2 for over 4 days before gradually dropping to zero in 6 days (**Figure 4b**). Under continuous illumination, the stability of the integrated system is maintained over a similar total time range (**Figure S9**). Refreshing the electrolyte reactivates the performance (**Figure S10**)

and X-ray photoelectron spectroscopy shows minor changes in the material other than slight oxidation of Pt (**Figure S11**), suggesting that the deactivation mechanism is coming from the consumption of electrolyte. A flow-cell configuration is then likely to assist the stability.

In this study, we demonstrated a framework for pursuing high current densities for a solar-driven device using photoelectrochemical HER coupled with GOR using silicon. By employing a low overpotential catalyst such as PtAu for GOR, which shows a low onset potential of 0.4 V vs. RHE electrochemically, the voltage requirements to couple with HER become substantially lowered compared to OWS. As a result, the PtAu/Si photoanode exhibits a low onset potential of -0.05 V vs. RHE and can be coupled with Pt/SiNW photocathode to achieve a photocurrent density of 6 mA/cm^2 and stability for over 4 days under no applied bias. This was a first demonstration of our concept of using a photochemical diode approach to drive the reaction at appreciable current densities.

ASSOCIATED CONTENT

Supporting Information.
The Supporting Information is available free of charge on the ACS Publications website.

Methods, additional experimental data including XPS, electrochemical and PEC data (PDF)

AUTHOR INFORMATION

Corresponding Author

Peidong Yang – Department of Chemistry, University of California, Berkeley, California 94720, United States; Department of Materials Science and Engineering, University of California, Berkeley, California 94720, United States; Chemical Sciences Division, Lawrence Berkeley National Laboratory, Berkeley, California 94720, United States; Liquid Sunlight Alliance, Lawrence Berkeley National Laboratory, Berkeley, California 94720, United States; Kavli Energy NanoScience Institute, Berkeley, California 94720, United States; Email: p_yang@berkeley.com

Authors

Jia-An Lin – Department of Chemistry, University of California, Berkeley, California 94720, United States; Liquid Sunlight Alliance, Lawrence Berkeley National Laboratory, Berkeley, California 94720, United States

Inwhan Roh – Department of Chemistry, University of California, Berkeley, California 94720, United States; Liquid Sunlight Alliance, Lawrence Berkeley National Laboratory, Berkeley, California 94720, United States

Author Contributions

⊥J. -A. L., I. R. contributed equally to this study.

Funding Sources

No competing financial interests have been declared.

Notes

The authors declare no competing financial interest.

ACKNOWLEDGMENT

This work was supported by Liquid Sunlight Alliance, which is supported by the US Department of Energy, Office of Science, Office of Basic Energy Sciences, Fuels from Sunlight Hub under award DE-SC0021266. J. -A. L. acknowledges the financial support from Taiwan Ministry of Education. We thank the nanofabrication facilities and entire staff in Marvell Nanofabrication Laboratory. We thank Dr. Hasan Celik and UC Berkeley's NMR facility in the College of Chemistry (CoC-NMR) for spectroscopic assistance. Instruments in the CoC-NMR are supported in part by NIH S10OD024998. Work at the Molecular Foundry was supported by the Offices of Science, Office of Basic Energy Sciences, of the U.S. Department of Energy under Contract No. DE-AC02-05CH11231. We thank Dr. Virgil Andrei for helpful discussion.

REFERENCES

(1) Chu, S.; Majumdar, A. Opportunities and Challenges for a Sustainable Energy Future. *Nature* **2012**, *488* (7411), 294–303. https://doi.org/10.1038/nature11475.

(2) Lewis, N. S.; Nocera, D. G. Powering the Planet: Chemical Challenges in Solar Energy Utilization. *Proc. Natl. Acad. Sci.* **2006**, *103* (43), 15729–15735. https://doi.org/10.1073/pnas.0603395103.

(3) Deng, J.; Su, Y.; Liu, D.; Yang, P.; Liu, B.; Liu, C. Nanowire Photoelectrochemistry. *Chem. Rev.* **2019**, *119* (15), 9221–9259. https://doi.org/10.1021/acs.chemrev.9b00232.

(4) Archer, D. *Global Warming: Understanding the Forecast, 2nd Edition: Understanding the Forecast*; Wiley, 2011.

(5) Tachibana, Y.; Vayssieres, L.; Durrant, J. R. Artificial Photosynthesis for Solar Water-Splitting. *Nat. Photonics* **2012**, *6* (8), 511–518. https://doi.org/10.1038/nphoton.2012.175.

(6) Kim, D.; Sakimoto, K. K.; Hong, D.; Yang, P. Artificial Photosynthesis for Sustainable Fuel and Chemical Production. *Angew. Chem. Int. Ed.* **2015**, *54* (11), 3259–3266. https://doi.org/10.1002/anie.201409116.

(7) Nozik, A. J. Photochemical Diodes. *Appl. Phys. Lett.* **1977**, *30* (11), 567–569. https://doi.org/10.1063/1.89262.

(8) Andrei, V.; Roh, I.; Yang, P. Nanowire Photochemical Diodes for Artificial Photosynthesis. *Sci. Adv.* **2023**, *9* (6), eade9044. https://doi.org/10.1126/sciadv.ade9044.

(9) Liu, C.; Gallagher, J. J.; Sakimoto, K. K.; Nichols, E. M.; Chang, C. J.; Chang, M. C. Y.; Yang, P. Nanowire–Bacteria Hybrids for Unassisted Solar Carbon Dioxide Fixation to Value-Added Chemicals. *Nano Lett.* **2015**, *15* (5), 3634–3639. https://doi.org/10.1021/acs.nanolett.5b01254.

(10) Liu, C.; Tang, J.; Chen, H. M.; Liu, B.; Yang, P. A Fully Integrated Nanosystem of Semiconductor Nanowires for Direct Solar Water Splitting. *Nano Lett.* **2013**, *13* (6), 2989–2992. https://doi.org/10.1021/nl401615t.
(11) Chowdhury, F. A.; Trudeau, M. L.; Guo, H.; Mi, Z. A Photochemical Diode Artificial Photosynthesis System for Unassisted High Efficiency Overall Pure Water Splitting. *Nat. Commun.* **2018**, *9* (1), 1707. https://doi.org/10.1038/s41467-018-04067-1.
(12) Ye, S.; Shi, W.; Liu, Y.; Li, D.; Yin, H.; Chi, H.; Luo, Y.; Ta, N.; Fan, F.; Wang, X.; Li, C. Unassisted Photoelectrochemical Cell with Multimediator Modulation for Solar Water Splitting Exceeding 4% Solar-to-Hydrogen Efficiency. *J. Am. Chem. Soc.* **2021**, *143* (32), 12499–12508. https://doi.org/10.1021/jacs.1c00802.
(13) Pan, L.; Kim, J. H.; Mayer, M. T.; Son, M.-K.; Ummadisingu, A.; Lee, J. S.; Hagfeldt, A.; Luo, J.; Grätzel, M. Boosting the Performance of Cu2O Photocathodes for Unassisted Solar Water Splitting Devices. *Nat. Catal.* **2018**, *1* (6), 412–420. https://doi.org/10.1038/s41929-018-0077-6.
(14) Verma, S.; Lu, S.; Kenis, P. J. A. Co-Electrolysis of CO2 and Glycerol as a Pathway to Carbon Chemicals with Improved Technoeconomics Due to Low Electricity Consumption. *Nat. Energy* **2019**, *4* (6), 466–474. https://doi.org/10.1038/s41560-019-0374-6.
(15) Yu, X.; dos Santos, E. C.; White, J.; Salazar-Alvarez, G.; Pettersson, L. G. M.; Cornell, A.; Johnsson, M. Electrocatalytic Glycerol Oxidation with Concurrent Hydrogen Evolution Utilizing an Efficient MoO_x/Pt Catalyst. *Small* **2021**, *17* (44), 2104288. https://doi.org/10.1002/smll.202104288.
(16) Luo, H.; Barrio, J.; Sunny, N.; Li, A.; Steier, L.; Shah, N.; Stephens, I. E. L.; Titirici, M. Progress and Perspectives in Photo- and Electrochemical-Oxidation of Biomass for Sustainable Chemicals and Hydrogen Production. *Adv. Energy Mater.* **2021**, *11* (43), 2101180. https://doi.org/10.1002/aenm.202101180.
(17) Li, T.; Harrington, D. A. An Overview of Glycerol Electrooxidation Mechanisms on Pt, Pd and Au. *ChemSusChem* **2021**, *14* (6), 1472–1495. https://doi.org/10.1002/cssc.202002669.
(18) Simões, M.; Baranton, S.; Coutanceau, C. Electrochemical Valorisation of Glycerol. *ChemSusChem* **2012**, *5* (11), 2106–2124. https://doi.org/10.1002/cssc.201200335.
(19) Yazdani, S. S.; Gonzalez, R. Anaerobic Fermentation of Glycerol: A Path to Economic Viability for the Biofuels Industry. *Curr. Opin. Biotechnol.* **2007**, *18* (3), 213–219. https://doi.org/10.1016/j.copbio.2007.05.002.
(20) Fan, L.; Ji, Y.; Wang, G.; Chen, J.; Chen, K.; Liu, X.; Wen, Z. High Entropy Alloy Electrocatalytic Electrode toward Alkaline Glycerol Valorization Coupling with Acidic Hydrogen Production. *J. Am. Chem. Soc.* **2022**, *144* (16), 7224–7235. https://doi.org/10.1021/jacs.1c13740.
(21) Fan, L.; Liu, B.; Liu, X.; Senthilkumar, N.; Wang, G.; Wen, Z. Recent Progress in Electrocatalytic Glycerol Oxidation. *Energy Technol.* **2021**, *9* (2), 2000804. https://doi.org/10.1002/ente.202000804.
(22) Liu, B.; Wang, G.; Feng, X.; Dai, L.; Wen, Z.; Ci, S. Energy-Saving H_2 Production from a Hybrid Acid/Alkali Electrolyzer Assisted by Anodic Glycerol Oxidation. *Nanoscale* **2022**, *14* (35), 12841–12848. https://doi.org/10.1039/D2NR02689A.
(23) Andrei, V.; Reuillard, B.; Reisner, E. Bias-Free Solar Syngas Production by Integrating a Molecular Cobalt Catalyst with Perovskite–BiVO4 Tandems. *Nat. Mater.* **2020**, *19* (2), 189–194. https://doi.org/10.1038/s41563-019-0501-6.
(24) Wang, G.; Wang, H.; Ling, Y.; Tang, Y.; Yang, X.; Fitzmorris, R. C.; Wang, C.; Zhang, J. Z.; Li, Y. Hydrogen-Treated TiO_2 Nanowire Arrays for Photoelectrochemical Water Splitting. *Nano Lett.* **2011**, *11* (7), 3026–3033. https://doi.org/10.1021/nl201766h.
(25) Yang, W.; Prabhakar, R. R.; Tan, J.; Tilley, S. D.; Moon, J. Strategies for Enhancing the Photocurrent, Photovoltage, and Stability of Photoelectrodes for Photoelectrochemical Water Splitting. *Chem. Soc. Rev.* **2019**, *48* (19), 4979–5015. https://doi.org/10.1039/C8CS00997J.
(26) Kim, T. W.; Choi, K.-S. Nanoporous $BiVO_4$ Photoanodes with Dual-Layer Oxygen Evolution Catalysts for Solar Water Splitting. *Science* **2014**, *343* (6174), 990–994. https://doi.org/10.1126/science.1246913.
(27) Tateno, H.; Chen, S.-Y.; Miseki, Y.; Nakajima, T.; Mochizuki, T.; Sayama, K. Photoelectrochemical Oxidation of Glycerol to Dihydroxyacetone Over an Acid-Resistant Ta:$BiVO_4$ Photoanode. *ACS Sustain. Chem. Eng.* **2022**, *10* (23), 7586–7594. https://doi.org/10.1021/acssuschemeng.2c01282.
(28) Verma, A. M.; Laverdure, L.; Melander, M. M.; Honkala, K. Mechanistic Origins of the PH Dependency in Au-Catalyzed Glycerol Electro-Oxidation: Insight from First-Principles Calculations. *ACS Catal.* **2022**, *12* (1), 662–675. https://doi.org/10.1021/acscatal.1c03788.
(29) Lertthahan, P.; Yongprapat, S.; Therdthianwong, A.; Therdthianwong, S. Pt-Modified Au/C Catalysts for Direct Glycerol Electro-Oxidation in an Alkaline Medium. *Int. J. Hydrog. Energy* **2017**, *42* (14), 9202–9209. https://doi.org/10.1016/j.ijhydene.2016.05.120.
(30) Seger, B.; Pedersen, T.; Laursen, A. B.; Vesborg, P. C. K.; Hansen, O.; Chorkendorff, I. Using TiO_2 as a Conductive Protective Layer for Photocathodic H_2 Evolution. *J. Am. Chem. Soc.* **2013**, *135* (3), 1057–1064. https://doi.org/10.1021/ja309523t.
(31) Boettcher, S. W.; Warren, E. L.; Putnam, M. C.; Santori, E. A.; Turner-Evans, D.; Kelzenberg, M. D.; Walter, M. G.; McKone, J. R.; Brunschwig, B. S.; Atwater, H. A.; Lewis, N. S. Photoelectrochemical Hydrogen Evolution Using Si Microwire Arrays. *J. Am. Chem. Soc.* **2011**, *133* (5), 1216–1219. https://doi.org/10.1021/ja108801m.
(32) Roh, I.; Yu, S.; Lin, C.-K.; Louisia, S.; Cestellos-Blanco, S.; Yang, P. Photoelectrochemical CO_2 Reduction toward Multicarbon Products with Silicon Nanowire Photocathodes Interfaced with Copper Nanoparticles. *J. Am. Chem. Soc.* **2022**, *144* (18), 8002–8006. https://doi.org/10.1021/jacs.2c03702.
(33) Kwon, Y.; Lai, S. C. S.; Rodriguez, P.; Koper, M. T. M. Electrocatalytic Oxidation of Alcohols on Gold in Alkaline Media: Base or Gold Catalysis? *J. Am. Chem. Soc.* **2011**, *133* (18), 6914–6917. https://doi.org/10.1021/ja200976j.
(34) Sheng, H.; Janes, A. N.; Ross, R. D.; Hofstetter, H.; Lee, K.; Schmidt, J. R.; Jin, S. Linear Paired Electrochemical Valorization of Glycerol Enabled by the Electro-Fenton Process Using a Stable NiSe2 Cathode. *Nat. Catal.* **2022**, *5* (8), 716–725. https://doi.org/10.1038/s41929-022-00826-y.
(35) Jolimaitre, E.; Delcroix, D.; Essayem, N.; Pinel, C.; Besson, M. Dihydroxyacetone Conversion into

Lactic Acid in an Aqueous Medium in the Presence of Metal Salts: Influence of the Ionic Thermodynamic Equilibrium on the Reaction Performance. *Catal. Sci. Technol.* **2018**, *8* (5), 1349–1356. https://doi.org/10.1039/C7CY02385E.
(36) Sánchez, B. S.; Gross, M. S.; Querini, C. A. Pt Catalysts Supported on Ion Exchange Resins for Selective Glycerol Oxidation. Effect of Au Incorporation. *Catal. Today* **2017**, *296*, 35–42. https://doi.org/10.1016/j.cattod.2017.05.082.
(37) Liu, D.; Liu, J.-C.; Cai, W.; Ma, J.; Yang, H. B.; Xiao, H.; Li, J.; Xiong, Y.; Huang, Y.; Liu, B. Selective Photoelectrochemical Oxidation of Glycerol to High Value-Added Dihydroxyacetone. *Nat. Commun.* **2019**, *10* (1), 1779. https://doi.org/10.1038/s41467-019-09788-5.
(38) Hwang, Y. J.; Hahn, C.; Liu, B.; Yang, P. Photoelectrochemical Properties of TiO_2 Nanowire Arrays: A Study of the Dependence on Length and Atomic Layer Deposition Coating. *ACS Nano* **2012**, *6* (6), 5060–5069. https://doi.org/10.1021/nn300679d.
(39) Liu, Y.; Wang, M.; Zhang, B.; Yan, D.; Xiang, X. Mediating the Oxidizing Capability of Surface-Bound Hydroxyl Radicals Produced by Photoelectrochemical Water Oxidation to Convert Glycerol into Dihydroxyacetone. *ACS Catal.* **2022**, *12* (12), 6946–6957. https://doi.org/10.1021/acscatal.2c01319.
(40) Long; Cai; Kisch, H. Visible Light Induced Photoelectrochemical Properties of N-$BiVO_4$ and n-$BiVO_4$/p-Co_3O_4. *J. Phys. Chem. C* **2008**, *112* (2), 548–554. https://doi.org/10.1021/jp075605x.
(41) Janczarek, M.; Kowalska, E. On the Origin of Enhanced Photocatalytic Activity of Copper-Modified Titania in the Oxidative Reaction Systems. *Catalysts* **2017**, *7* (11), 317. https://doi.org/10.3390/catal7110317.
(42) Chen, S.; Wang, L.-W. Thermodynamic Oxidation and Reduction Potentials of Photocatalytic Semiconductors in Aqueous Solution. *Chem. Mater.* **2012**, *24* (18), 3659–3666. https://doi.org/10.1021/cm302533s.
(43) Persson, C.; Lindefelt, U.; Sernelius, B. E. Band Gap Narrowing in *n* -Type and *p* -Type 3C-, 2H-, 4H-, 6H-SiC, and Si. *J. Appl. Phys.* **1999**, *86* (8), 4419–4427. https://doi.org/10.1063/1.371380.
(44) Vargas-Barbosa, N. M.; Geise, G. M.; Hickner, M. A.; Mallouk, T. E. Assessing the Utility of Bipolar Membranes for Use in Photoelectrochemical Water-Splitting Cells. *ChemSusChem* **2014**, *7* (11), 3017–3020. https://doi.org/10.1002/cssc.201402535.
(45) Luo, J.; Vermaas, D. A.; Bi, D.; Hagfeldt, A.; Smith, W. A.; Grätzel, M. Bipolar Membrane-Assisted Solar Water Splitting in Optimal PH. *Adv. Energy Mater.* **2016**, *6* (13), 1600100. https://doi.org/10.1002/aenm.201600100.
(46) Vermaas, D. A.; Wiegman, S.; Nagaki, T.; Smith, W. A. Ion Transport Mechanisms in Bipolar Membranes for (Photo)Electrochemical Water Splitting. *Sustain. Energy Fuels* **2018**, *2* (9), 2006–2015. https://doi.org/10.1039/C8SE00118A.
(47) McDonald, M. B.; Ardo, S.; Lewis, N. S.; Freund, M. S. Use of Bipolar Membranes for Maintaining Steady-State PH Gradients in Membrane-Supported, Solar-Driven Water Splitting. *ChemSusChem* **2014**, *7* (11), 3021–3027. https://doi.org/10.1002/cssc.201402288.
(48) Palik, E. D.; Faust, J. W.; Gray, H. F.; Greene, R. F. Study of the Etch-Stop Mechanism in Silicon. *J. Electrochem. Soc.* **1982**, *129* (9), 2051–2059. https://doi.org/10.1149/1.2124367.
(49) Ali-Löytty, H.; Hannula, M.; Valden, M.; Eilert, A.; Ogasawara, H.; Nilsson, A. Chemical Dissolution of Pt(111) during Potential Cycling under Negative PH Conditions Studied by Operando X-Ray Photoelectron Spectroscopy. *J. Phys. Chem. C* **2019**, *123* (41), 25128–25134. https://doi.org/10.1021/acs.jpcc.9b05201.

Table of Contents